Int. J. Heat Mass Transfer. Vol. 36, No. 7, pp. 1833–1844, 1993
Printed in Great Britain

0017-9310/93 $6.00 + 0.00
© 1993 Pergamon Press Ltd

An interface tracking method applied to morphological evolution during phase change

W. SHYY, H. S. UDAYKUMAR and S.-J. LIANG
Department of Aerospace Engineering, Mechanics and Engineering Science, University of Florida, Gainesville, FL 32611, U.S.A.

(*Received* 17 *February* 1992 *and in final form* 27 *July* 1992)

Abstract—The focus of this work is the numerical simulation of interface motion during solidification of pure materials. First, we assess the applicability of the oft-used quasi-stationary approximation for interface motion. Such an approximation results in poor accuracy for non-trivial Stefan numbers. Next, a generic interface tracking procedure is designed, which overcomes restrictions of single-valuedness of the interface imposed by commonly used mapping methods. This method incorporates with ease interface phenomena involving curvature, which assume importance at the smaller scales of a deformed interface. The method is then applied to study the development of a morphologically unstable phase interface. The issue of appropriate scaling has been addressed. The Gibbs–Thomson effect for curved interfaces has been included. The evolution of the interface, with the competing mechanisms of undercooling and surface tension is found to culminate in tip-splitting, cusp formation and persistent cellular development.

1. INTRODUCTION

WITH INCREASING demand for high-quality materials produced at economically viable rates, the physics involved in their processing has received considerable attention from the fluid mechanics and materials science communities. The objective is to understand and hence control the thermofluid aspects of the phase change process, in order to obtain desired impurity concentration distributions and structural uniformity. Apart from its economic significance, the study of the solidification process has also been viewed as a means to unearth a paradigm for 'pattern formation' in nature [1, 2]. The fundamental issue to be resolved is how such qualitatively reproducible patterns emerge from the apparently random field resulting from the diffusion process.

Analytical treatments of the complete diffusion problem encounter nonlinearities and non-locality associated with motion of the deformed interface separating the two phases. This is a descendent of the Stefan problem [3] of considerable mathematical interest. Computation of the motion of the phase interface in the complete diffusional form have been made, for example, by Brush and Sekerka [4] for crystal growth and for the analogous Saffman–Taylor problem, by DeGregoria and Schwartz [5]. While the former use a finite difference approach with a mapping method, the latter employ the boundary element technique. Finite element methods have also been frequently used [6, 7] to capture the deformed interfaces.

Under suitable conditions, instability of the phase interface ultimately leads to a highly branched, dendritic structure [1, 8]. Competing mechanisms determine such characteristics of the dendrite as wavelength of the primary instability, the radius at the tip of the paraboloidal primary dendrite, the emergence of side-branches, and side-branch spacing. While the supercooling of the melt destabilises in the sense that a small outward bump on the solid will grow, surface tension stabilises by establishing a short wavelength cutoff. The preferred orientations of the dendrites and the side-branching activity are believed to be controlled 'microscopically' by the anisotropy that naturally prevails in a crystal lattice [8]. Thus, from the geometry and physical mechanisms involved, it is obvious that a faithful simulation of morphological evolution is predicated on accurate computation of the location and curvature of the phase change front.

Among the methods proposed in the literature to track moving fronts [3, 9] one commonly used approach [4, 10, 11] involves coordinate transformation to map the irregularly shaped physical domain onto a regular computational domain. The solutions may then be obtained in the transformed domain and the interface position updated. Often a further simplification is made by assuming that the time scale for interfacial motion is long compared to thermal relaxation times. This justifies dropping terms representing grid movement from the equations governing interface motion [10, 11]. This procedure is termed quasi-stationary and is appropriate for slow-moving interfaces.

Hitherto, simulations of phase change found little need for the curvature-dependent interface temperature condition, the Gibbs–Thomson effect [12], since in capturing the global shape of the phase boundary, the local curvatures are not significant. However, if one is interested in resolving the microstructure resulting from the phase change, then it is

NOMENCLATURE

c_p	specific heat
d_0	capillary length
F	dimensionless function defining interface
H	characteristic length scale
J	inverse Jacobian of transformation
k	thermal conductivity
l_T	diffusion length
L	latent heat of fusion
$\mathbf{n}$	unit normal vector to interface, pointing toward the cold direction
n	dimensional normal coordinate
t	dimensional time
T	dimensional temperature
$s(y, t)$	dimensional function defining interface
$S(Y, t^*)$	dimensionless function defining interface
St	Stefan number
v_{ext}	velocity scale of outer region
V_N	normal velocity of interface
(x, y, t)	physical coordinates
(X, Y, t^*)	non-dimensional physical coordinates.

Greek symbols

α	thermal diffusivity
γ	dimensional surface tension
γ_{eff}	effective surface tension
θ	dimensionless temperature
κ	curvature
λ	root of equation (10)
λ_c	instability wavelength
ν	inner region velocity scale
(ξ, η, τ)	transformed coordinates
ρ	dimensional density
τ	dimensionless time
ψ	arc length along interface.

Superscripts

*	non-dimensional quantity.

Subscripts

l	liquid
s	solid
eq	equilibrium
interface	interface value
m	melting point.

well known from morphological stability theory [1] that microscopic mechanisms hold the key to a description of instabilities. This distinction in computational requirements arises due to the length scales of the morphological features. In the well-investigated material succinonitrile (SCN) [13], for instance, the instability length (the wavelength selected) is in the range of microns. The diffusion length, i.e. the distance over which the thermal field relaxes is of the order of millimetres. Thus, on a macroscopic scale, the global phase change front is virtually unaffected by morphological instabilities. However, the all-important microstructure of the crystal is controlled by the interfacial phenomena. Thus, there is a need to bridge the gap between (i.e. to match) the two disparate thermal fields and interfacial behaviour.

In the present work, we first seek to assess the impact of a quasi-stationary approximation on the accuracy of numerical solutions. This is the content of Section 2. In Section 3, we reformulate the interface treatment to avoid the restriction to non-branched and isothermal interfaces inherent in most methods currently in use [10, 11]. The computational procedure developed is then applied to compute the motion of deformed interfaces. In Section 4, we introduce the scaling appropriate to a physically realistic thermal field in which the interface morphology develops. It will be shown that such scaling is applicable to the inner region, i.e. to the instability events at the small scales. The method will then be applied to illustrate the competition among the mechanisms affecting stability, such as surface tension and thermal diffusion.

2. ASSESSMENT OF THE QUASI-STATIONARY APPROXIMATION

For a pure conduction problem with phase change between liquid and solid, the governing equations, in dimensional form, for the energy transfer and interface movement are, respectively [3],

$$\frac{\partial T_i}{\partial t} = \alpha_i\left(\frac{\partial^2 T_i}{\partial x^2} + \frac{\partial^2 T_i}{\partial y^2}\right), \quad i = 1, s \tag{1}$$

$$\rho L \frac{\partial s}{\partial t} = -k_l \frac{\partial T_l}{\partial n} + k_s \frac{\partial T}{\partial n}. \tag{2}$$

The partials with respect to n represent derivatives in the direction of the local normal to the interface. The following non-dimensionalizing procedure is adopted: $X = x/H$, $Y = y/H$, $S = s/H$, H being a representative length scale to be chosen for the specific problem studied, $t^* = \alpha_l t/H^2$, $\rho^* = \rho/\rho_l$ and $\theta = (T - T_m)/(T_\infty - T_m)$, where T_m and T_∞ are, respectively, the melting temperature and the imposed temperature at the appropriate boundary. Consider heat transport in the liquid phase only. Then, equations (1) and (2), discarding the subscript, become:

$$\frac{\partial \theta}{\partial t^*} = \frac{\partial^2 \theta}{\partial X^2} + \frac{\partial^2 \theta}{\partial Y^2} \tag{3}$$

$$-\frac{\partial \theta}{\partial n^*} = \frac{\rho^*}{St}\frac{\partial S}{\partial t^*} \tag{4}$$

where $St = c_p(T_\infty - T_m)/L$ is the Stefan number.

If $X = S(Y, t)$, then equation (4) specialised to an isothermal interface, can be rewritten as

$$\left[1+\left(\frac{\partial S}{\partial Y}\right)^2\right]\frac{\partial \theta}{\partial X} = -\frac{\rho^*}{St}\frac{\partial S}{\partial t^*}. \tag{5}$$

Following the transformation from Cartesian (X, Y, t) to curvilinear (ξ, η, τ) coordinates [14], such that $X = X(\xi, \eta, \tau)$, $Y = Y(\xi, \eta, \tau)$ and $t^* = \tau$, equations (3) and (4) become:

$$\theta_\tau + \frac{1}{J}(X_\eta Y_\tau - Y_\eta X_\tau)\theta_\xi + \frac{1}{J}(Y_\xi X_\tau - X_\xi Y_\tau)\theta_\eta$$

$$= \frac{1}{J}\left[\frac{1}{J}(q_1\theta_\xi - q_2\theta_\eta)\right]_\xi + \frac{1}{J}\left[\frac{1}{J}(-q_2\theta_\xi + q_3\theta_\eta)\right]_\eta \tag{6a}$$

$$\frac{1}{J}[(Y_\eta\theta)_\xi - (Y_\xi\theta)_\eta]\left[1+\left(\frac{1}{J}[-(X_\eta S)_\xi + (X_\xi S)_\eta]\right)^2\right] = -\frac{\rho}{St}\left[\frac{\partial S}{\partial \tau} + \frac{1}{J}(X_\eta Y_\tau - Y_\eta X_\tau)S_\xi + \frac{1}{J}(Y_\xi X_\tau - X_\xi Y_\tau)S_\eta\right] \tag{6b}$$

where

$$\begin{aligned} q_1 &= X_\eta^2 + Y_\eta^2, \\ q_2 &= X_\xi X_\eta + Y_\xi Y_\eta, \\ q_3 &= X_\xi^2 + Y_\xi^2, \\ J &= X_\xi Y_\eta - X_\eta Y_\xi. \end{aligned} \tag{7}$$

Equations (6a) and (6b) constitute the complete set of the equations in the generalised coordinates for energy transfer and interface movement. In the course of the computations, at every time step, both equation (6a) and (6b) need to be iteratively updated until they are simultaneously satisfied everywhere in the domain. Standard second-order central differences are used for all spatial derivatives. The quasi-stationary approach adopted by many researchers, e.g. [10, 11], simplifies the above equations by dropping all the terms involving coordinate movement, i.e. X_τ, Y_τ. To test whether such a simplification is acceptable, we design a situation where the interface moves as a planar front. In addition, the temperature in the solid is considered uniform. Thus the heat transport is effectively one-dimensional and occurs in the liquid phase only. Boundary and initial conditions are therefore given by [3],

B.C.

$$\begin{aligned} &\theta = 1, \quad X = 0, \quad \tau \geqslant 0 \\ &\theta = 0, \quad X \geqslant S, \quad \tau \geqslant 0 \end{aligned} \tag{8}$$

I.C.

$$\theta(X, \tau = 0.1) = 1 - \frac{\operatorname{erf}\left(\dfrac{X}{2\sqrt{0.1}}\right)}{\operatorname{erf}(\lambda)}$$

$$S(X, \tau = 0.1) = 2\lambda\sqrt{0.1} \tag{9}$$

where λ is the root of the following equation

$$\lambda\, e^{\lambda^2}\operatorname{erf}(\lambda) = \frac{St}{\sqrt{\pi}}. \tag{10}$$

The exact solution [3] for equations (3) and (4), with $\rho^* = 1$, with the boundary and initial conditions given in equations (8) and (9) is

$$\theta = 1 - \frac{\operatorname{erf}\left(\dfrac{X}{2\sqrt{\tau}}\right)}{\operatorname{erf}(\lambda)}. \tag{11}$$

Two numerical solution procedures are designed to compare the solutions obtained from the complete form of equations (6a) and (6b) and the quasi-stationary form:

(1) Full treatment: a standard procedure involving backward Euler time stepping along with a second-order central difference spatial discretization scheme is used to solve equations (6a) and (6b). This full set of equations is solved iteratively in a coupled manner to continually update the nonlinear coefficients resulting from the coordinate movement and transformation.

(2) Quasi-stationary treatment: by invoking the quasi-stationary assumption, coordinate movement terms are neglected. On dropping the grid movement terms, the equations governing energy transfer and interface movement are decoupled and only a simple explicit procedure is needed to update the interface location.

Three values of the Stefan number were chosen to test the performance of the above two numerical approaches. Eleven grid points are used along the x-direction in each case. For small St, i.e. 0.1303, as seen in Fig. 1(a), both full and quasi-stationary solutions are in close agreement with the exact solution in terms of the interface trajectory as well as the temperature profile, although the full approach is marginally superior. However, as expected, with increasing St the quality of solutions obtained from the quasi-stationary method is progressively degraded. In contrast, good agreement is maintained between the solutions of the full approach and the exact solution. Although the Stefan number observed from many naturally occurring processes is small, for some problems of current technological significance, such as the continuous ingot casting of metal alloys [15], Stefan numbers of order 1 are commonly encountered. Obviously, with a low St, the interface velocity is modest, and neglecting grid movement terms does not impact significantly on the numerical accuracy. As St

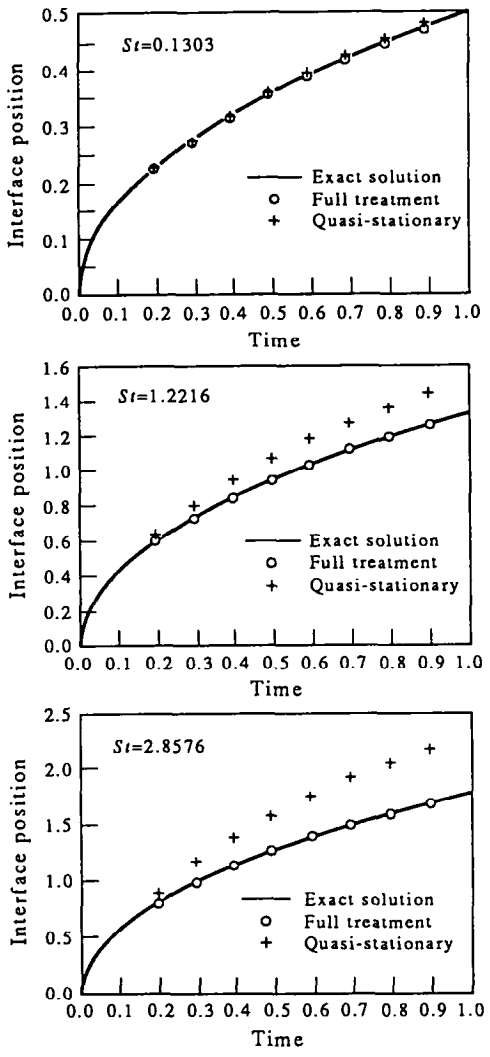

FIG. 1. Comparison of trajectories predicted by the full equations and the quasi-stationary equations with exact solution, for three values of Stefan number.

becomes larger, however, the simplification to the quasi-stationary approach is no longer acceptable.

3. A GENERAL PROCEDURE FOR INTERFACE TRACKING

As mentioned in Section 2, equations (6a) and (6b) apply only to an isothermal interface. Also, the construction of those equations precludes the possibility of capturing branched interfaces. As a first step towards overcoming this difficulty, an alternate interface treatment is designed as follows. Consider the equation for interface advance,

$$-\frac{\rho^*}{St} V_N^* = \left[\frac{\partial\theta}{\partial n_l^*} - \frac{k_s}{k_l}\frac{\partial\theta}{\partial n_s^*}\right]. \tag{12}$$

The local normal to the interface is given by,

$$\mathbf{n} = \frac{1}{|\nabla F|}\left(\frac{\partial F}{\partial X}\mathbf{i} + \frac{\partial F}{\partial Y}\mathbf{j}\right) \tag{13}$$

where $F = F(X, Y, t^*)$ is the curve defining the interface. The interface shape is defined in a piecewise fashion to facilitate handling of branched interfaces. Here a quadratic polynomial fit is performed for three successive nodal points at each point of the interface. Thus, at the ith point on the interface we designate the curve,

$$Y_i = a_i X_i^2 + b_i X_i + c_i,$$

$$\text{i.e. } F_i = Y_i - (a_i X_i^2 + b_i X_i + c_i)$$

defines the interface.

The a_i, b_i and c_i are determined from the known values (X_j, Y_j), $j = i-1$, i, $i+1$. The choice of the piecewise approximating polynomial is not restricted to the parabolic form. In fact, using circular arc elements is more convenient for handling multiple-valued interfaces and is in use in ongoing work. The local curve definition yields the deriatives (F_x, F_y and F_{xx}) at each point on the interface. Thus the the curvature at each point is obtained from,

$$\kappa^* = \frac{Y_{XX}}{(1+Y_X^2)^{3/2}}. \tag{14}$$

We may write equation (12) as,

$$-\frac{\rho^*}{St} V_N^* = \frac{1}{|\nabla F|}[(F_X\theta_X + F_Y\theta_Y)_l - (F_X\theta_X + F_Y\theta_Y)_s]. \tag{15}$$

In computing the interface normal velocity then, one seeks to obtain the derivatives F_x, F_y and θ_x, θ_y. The derivatives of temperature may be obtained in the transformed coordinates itself. F_x and F_y of course are directly available in the physical domain from the curve fit. Thus the new coordinates of the interfacial points are obtained from:

$$X^{n+1} = X^n + \frac{\partial F}{\partial X}\frac{V_N^*}{|\nabla F|}\delta t^* \tag{16a}$$

$$Y^{n+1} = Y^n + \frac{\partial F}{\partial Y}\frac{V_N^*}{|\nabla F|}\delta t^* \tag{16b}$$

where δt^* is the time step size. Having obtained these new coordinates of the curve, the thermal field is solved for once again, the curve fit is performed at the interface and a fresh interface position is obtained from equations (16a) and (16b). All these procedures are performed in a fully coupled manner involving interaction among the temperature field, interface motion and grid movement at each iteration. This alternative interface treatment is compared firstly with the results of Section 2, where the thermal field is active in the liquid region only. The boundary conditions are given by equation (8). From Figure 2 it is evident that for all three Stefan numbers tried, namely, 0.1303, 1.2216 and 2.8576, the accuracy of the present scheme is satisfactory and comparable to those in

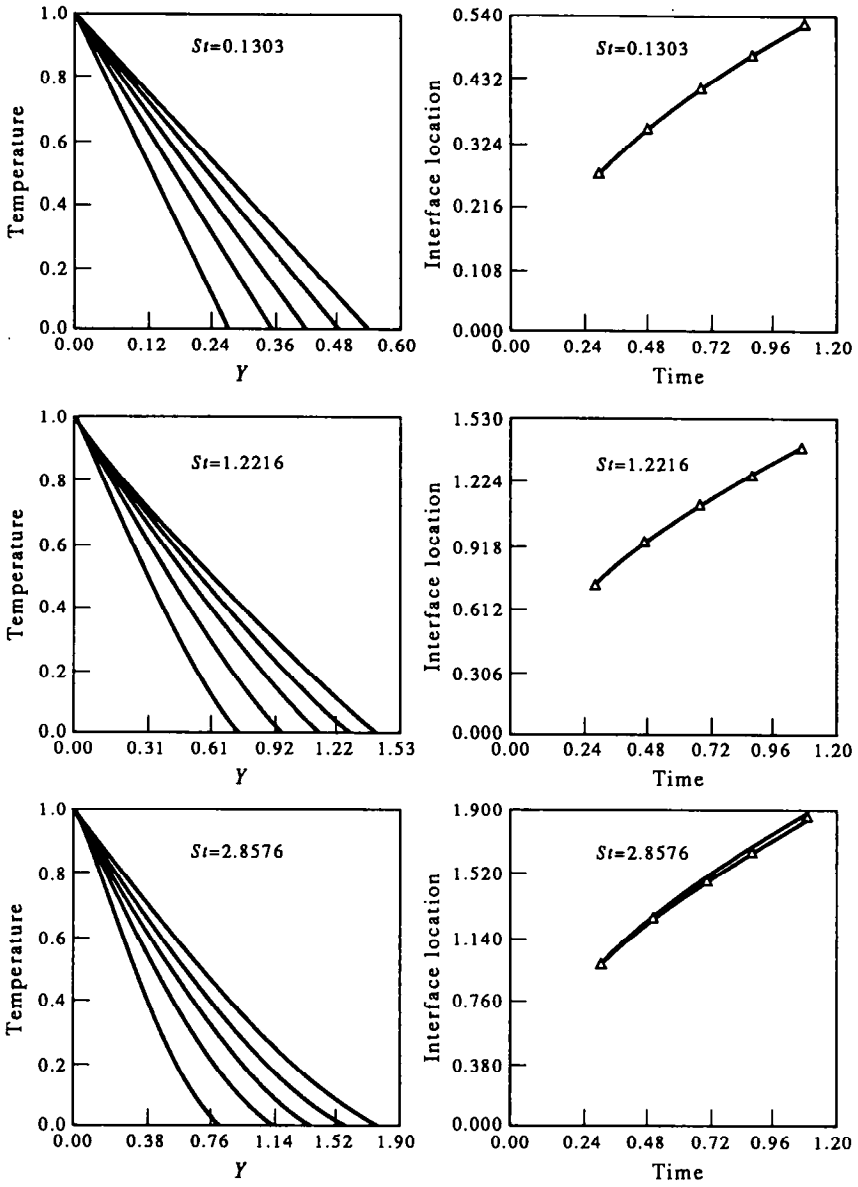

FIG. 2. Comparison of computed and exact solutions for $St = 0.1303$, $St = 1.2216$ and $St = 2.8576$. The respective Stefan numbers are shown in the boxes. (a) Exact and computed temperature fields at different time instants. (b) Superposed exact and computed interface locations vs time.

Section 1, Fig. 1. As can be seen, the computed and exact temperature fields are in excellent agreement.

4. MOTION OF CURVED FRONTS

The interface tracking method developed in Section 3 is now applied to follow the development of the phase change front from long enough times to obtain substantial curvature of an initially slightly perturbed interface. Physically, when the phase interface is deformed surface tension seeks to round out regions of strong curvature. This effect is expressed, for an interface in thermodynamic equilibrium (i.e. for sufficiently slow moving interfaces) by the Gibbs–Thomson formula,

$$T_{\text{interface|eq}} = T_m\left(1 - \frac{\gamma\kappa}{L}\right). \tag{17}$$

T_m is the melting temperature of a flat interface. $T_{\text{interface|eq}}$ is the modified temperature after accounting for the Gibbs–Thomson effect, and in this form is applicable to an interface in chemical equilibrium. Thus, surface tension γ acts to lower the temperature of regions of strong positive curvature, hence exerting a stabilising influence. Here, κ is the local curvature

of the front. In reality, the lattice of the growing crystal imposes a directional dependence on the value of the surface tension [16]. Then γ becomes a function of ϕ, the angular deviation of the local normal at the interface from the growth axis. In summary, equations (1), (2) and (17) provide a complete set of equations governing motion of curved interfaces under the assumption that the interface kinetics is infinitely fast compared to the time scales of diffusion and interfacial motion.

A procedure for scaling

(i) *Inner region.* For the phase change problem, in the absence of convection, two length scales are obtained. $l_T = 2\alpha/V_N$, is the thermal diffusion length, and $d_0 = \gamma/L$, is the capillary length. Linear stability analysis [1] of a planar interface indicates that the critical wavelength for morphological stability is given by,

$$\lambda_c = O(\sqrt{d_0 l_T}). \tag{18}$$

Thus the instability wavelength lies in the range of microns. Therefore three distinct scales can be defined. The only length scale that is a property of the material is the capillary length d_0 $(=\gamma L)$. In practice the sole parameter that is externally controlled for solidification from a pure melt is the melt undercooling Δ. The front velocity for a planar front is then a function of Δ and the size of the domain. In tracking the morphological development of the interface the length scale of concern is the instability wavelength λ_c, which will be adopted as our length scale. Let us define the region at the scale of λ_c as the inner region and that corresponding to l_T as the outer region (here we shall take $\lambda_c = \sqrt{(d_0 l_T)}$).

Figure 3 illustrates the situation resulting from the differences in scale that we encounter in morphological stability phenomena. From the figure, it is clear that the temperature variations faced by the region adjoining the front are of order $\Delta\lambda_c/l_T$ $(\ll\Delta)$ and not Δ. An appropriate choice of scaling parameters has been found to be critical for computational efficiency. Adopting a temperature scale Δ results in extremely slow computational development of the front due to the resulting small values of non-dimensional velocities [5]. Thus, with the scales decided upon above, the equation for velocity of the interface becomes,

$$\rho L v V_N^* = \frac{\rho\alpha_l c_{pl}\Delta\lambda_c}{\lambda_c l_T}\left(-\frac{\partial\theta}{\partial n_l^*} + \frac{k_s}{k_l}\frac{\partial\theta}{\partial n_s^*}\right). \tag{19}$$

Here, V_N^* is the dimensionless velocity, and v is the reference velocity scale. For $O(1)$ front velocity, we obtain the velocity scale, $r = O(St\,(\alpha_l/l_T))$, where St is again the Stefan number.

The equation then becomes, in non-dimensional form,

$$V_N^* = \left(-\frac{\partial\theta}{\partial n_l^*} + \frac{k_s}{k_l}\frac{\partial\theta}{\partial n_s^*}\right). \tag{20}$$

The form of the governing equation adopted depends on the scaling procedure applied. Hence, although equations (4) and (20) for the interfacial velocity were obtained from the same dimensional equation, equation (2), they differ in appearance. The choice of length, time and velocity scales and the resulting governing equations have substantial implications in terms of computational efficiency.

Thus the time scale of motion of the interface is,

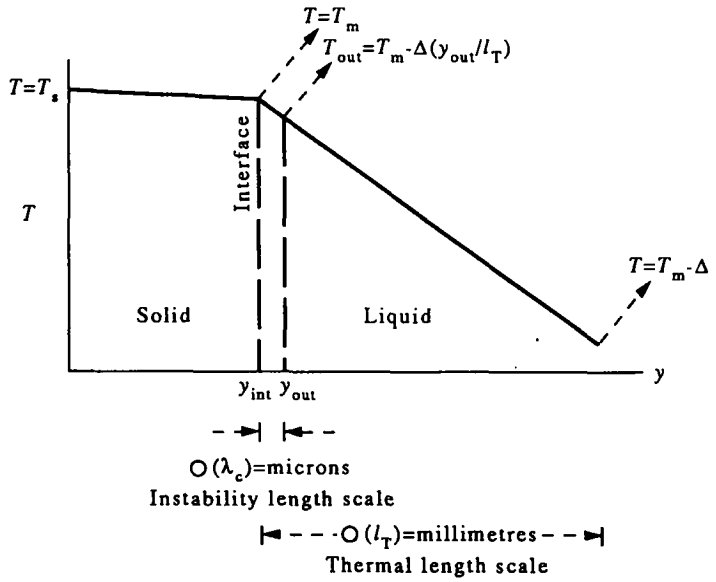

FIG. 3. Illustration of a typical temperature distribution for the configuration in Fig. 4. The relevant temperature and length scales are indicated.

$$\Im = \frac{\lambda_c}{v} = \frac{\lambda_c l_T}{\alpha_l St}. \quad (21)$$

Hence the dimensionless form of equation for heat conduction is,

$$\varepsilon_1 St\, \theta_\tau = \nabla^2 \theta \quad (22)$$

where $\varepsilon_1 = \lambda_c/l_T \ll 1$. Hence, to first-order the inner temperature field is governed by the Laplace equation and not the unsteady diffusion equation. The diffusion equation is relevant to the interfacial processes only when $St = O(1/\varepsilon_1)$ i.e. when the undercooling is large enough in comparison to L/c_p and the size scale of instability becomes comparable to the diffusion length.

We may now write the following expression for the non-dimensionalised interfacial temperature which is obtained from equation (17),

$$\theta_{\text{interface|eq}} = \theta_m\left(1 - \frac{d_0\gamma^*(\phi)\kappa^*}{\lambda_c}\right)$$

$$= \theta_m(1 - \varepsilon_2\gamma^*(\phi)\kappa^*) \quad (23)$$

where the superscripts * indicate non-dimensional quantities and $\varepsilon_2 = d_0/\lambda_c$. The curvature has been non-dimensionalised in terms of $(1/\lambda_c)$. We designate $\varepsilon_2\theta_m\gamma^*$ as γ_{eff}, the effective surface tension for our problem. Figure 4 illustrates the physical domain on which we carry out our computations and the boundary conditions applied. In actuality, the boundary conditions at $y = y_{\text{out}}$ and $y = 0$ are to be obtained from a matching procedure from the external field.

(ii) *Outer region.* As far as the outer region is concerned, the interface is to leading order merely a planar front. The temperature scale appropriate to the outer region is Δ, the undercooling. Lengths scale like $l_T = 2\alpha_l/v_{\text{ext}}$, the diffusion length, where v_{ext} is the typical velocity of the planar front as viewed from the outer scales. The outer time scale may thus be taken to be l_T^2/α_l. Conditions corresponding to the imposed undercooling apply at the boundaries of the external field. In the results to follow, a further assumption is made that the interfacial motion is slow enough so that the temperature linearly relaxes to $T_m - \Delta$ over a distance l_T, the diffusion length.

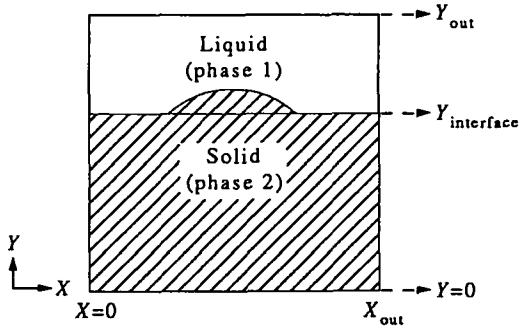

FIG. 4. Schematic of the physical domain.

Therefore, as in Fig. 3, at distance y_{out} from the interface,

$$T_{\text{l|inner}} = T_m - \left(\frac{y_{\text{out}}}{l_T}\right)\Delta. \quad (24)$$

Non-dimensionalising, one obtains the temperature at y_{out} as,

$$\theta_{\text{l|inner}} = \theta_m - Y_{\text{out}} \quad (25)$$

where $Y_{\text{out}} = y_{\text{out}}/\lambda_c$ according to the scales adopted. Hence this value of temperature is specified at the boundary at $Y = Y_{\text{out}}$.

Features of the computational method

Equations (20–23) are solved to follow the motion of a curved interface in the inner region. The coupled-implicit treatment along with the generalised interface update procedure is used. A small perturbation is placed on the interface, and a steady-state temperature field is taken as the initial condition. Temperature boundary conditions as applied as described above at $Y = 0$, i.e. the solid boundary and at $Y = Y_{\text{out}}$, the liquid boundary. At the sides of the domain we continue to impose an adiabatic boundary condition. Due to the assumed symmetry, the interface is constrained to remain normal to the boundaries at $X = 0$ and $X = X_{\text{out}}$. Hence, at the boundaries, $F_x = 0$.

An adaptively generated grid distributes grid points in the desired regions. This may be accomplished by spacing the points appropriately along the interface as follows [17]: let w_i be a weight function corresponding to the ith point along the interface, given by,

$$w_i = \left(1 + \frac{\omega\kappa_i^2}{\kappa_{\max}^2}\right) \quad (26)$$

where $\kappa_{\max}$ is the maximum value of the curvature along the interface, and ω is an adjustable parameter. The arc length at any node i, is computed based on the equal variation of $1/w$.

It is well known in dendritic growth theory [1] that the tip of the dendrite plays a crucial and sensitive role in determining its structure, in regard to wavelength and velocity selection. Thus it is desirable to place grid points preferentially at the tip by modifying the constant ω suitably [5]. This procedure is adopted in our calculations below. ω is assigned the value 0.5 when $\kappa_i > 0$ and 0.1 when $\kappa_i < 0$.

Results and discussion

The development of a perturbed interface, on the scale of the inner region, was tracked first for the case of zero surface tension. The initial perturbation of the interface was applied in the form of a cosine wave. The form of the perturbation was, $Y_i = Y_{\text{interface}}(1 - 0.05\cos(\pi X_i/X_{\text{out}}))$. Symmetry was

assumed and hence only half of the perturbation was treated. Forty-one grid points along X-direction, and along Y 101 grid points in the liquid and 41 points in the solid are used in the calculations.

The width of the domain for computation is taken to be four (lengths being non-dimensionalised by λ_c), which is the half-wavelength of the disturbance. The height Y_{out} is taken to be 50. The interface is orginally positioned at $Y_{interface} = 10$. The amplitude of perturbation is small, being 0.0125 times the wavelength. At the liquid boundary, in accordance with the scaling discussed above, dimensionless temperature of $\theta - \theta_m = -40$ is applied, while at the solid boundary at $Y = 0$, $\theta - \theta_m = 1$. Thus the perturbation faces an undercooled melt, and the Mullins–Sekerka instability [1] mechanism must operate.

The results for the zero surface tension case, in Fig. 5, show the rapid development of the instability

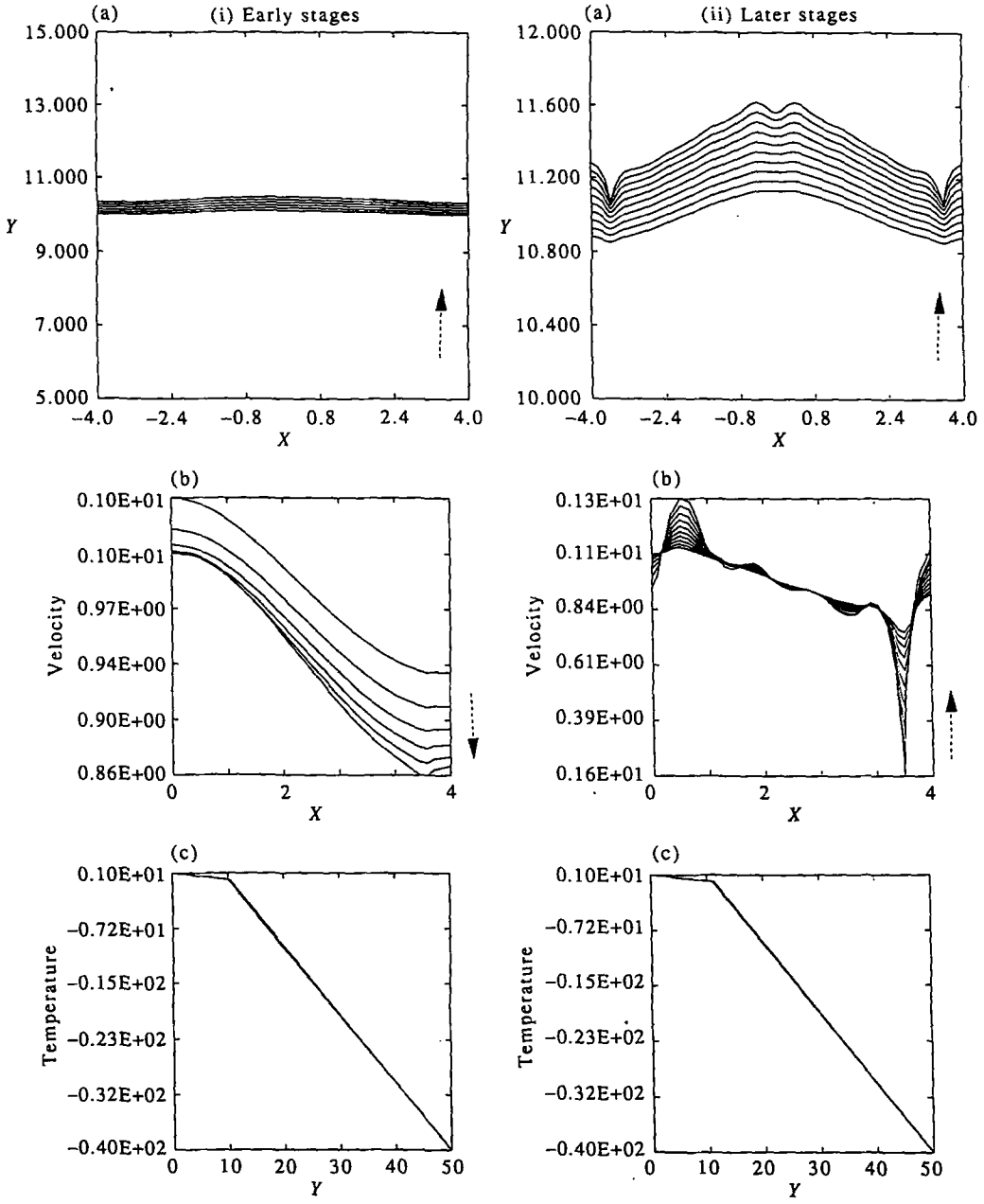

FIG. 5. Development of perturbed interface without surface tension. Arrows show sequence of development. Only the right half was calculated. (i) Early stages of growth: (a) interface shape after reflection of the half computed. (b) Velocity of the right half. (c) Temperature profile at $X = 2$ in the two phases. (ii) Later stages of growth. (a), (b) and (c) as above.

leading to the splitting of the tip of the proturberance and the formation of a cusp near the boundary. This is consistent with the theory of travelling isothermal fronts (or isobaric fronts in the case of Saffman–Taylor fingers [5, 17]). It is found that in such cases, depending on the initial conditions, the disturbance may bifurcate via tip-splitting or may sharpen into cusps. This is due to the fact that in the absence of surface tension, there is no physical mechanism that provides the short-wave cutoff. The lower limit of resolvable scales is set computationally by the grid spacing. Thus, all scales below the single available length scale, namely l_T down to the grid spacing are permissible: The initial amplitude to wavelength ratio for the given perturbation, shown in Fig. 5(ia) is 0.0125. At the final instant shown in Fig. 5(iia) the protuberance has grown to just eight times its initial amplitude. On the left, in Fig. 5(ia), is shown the

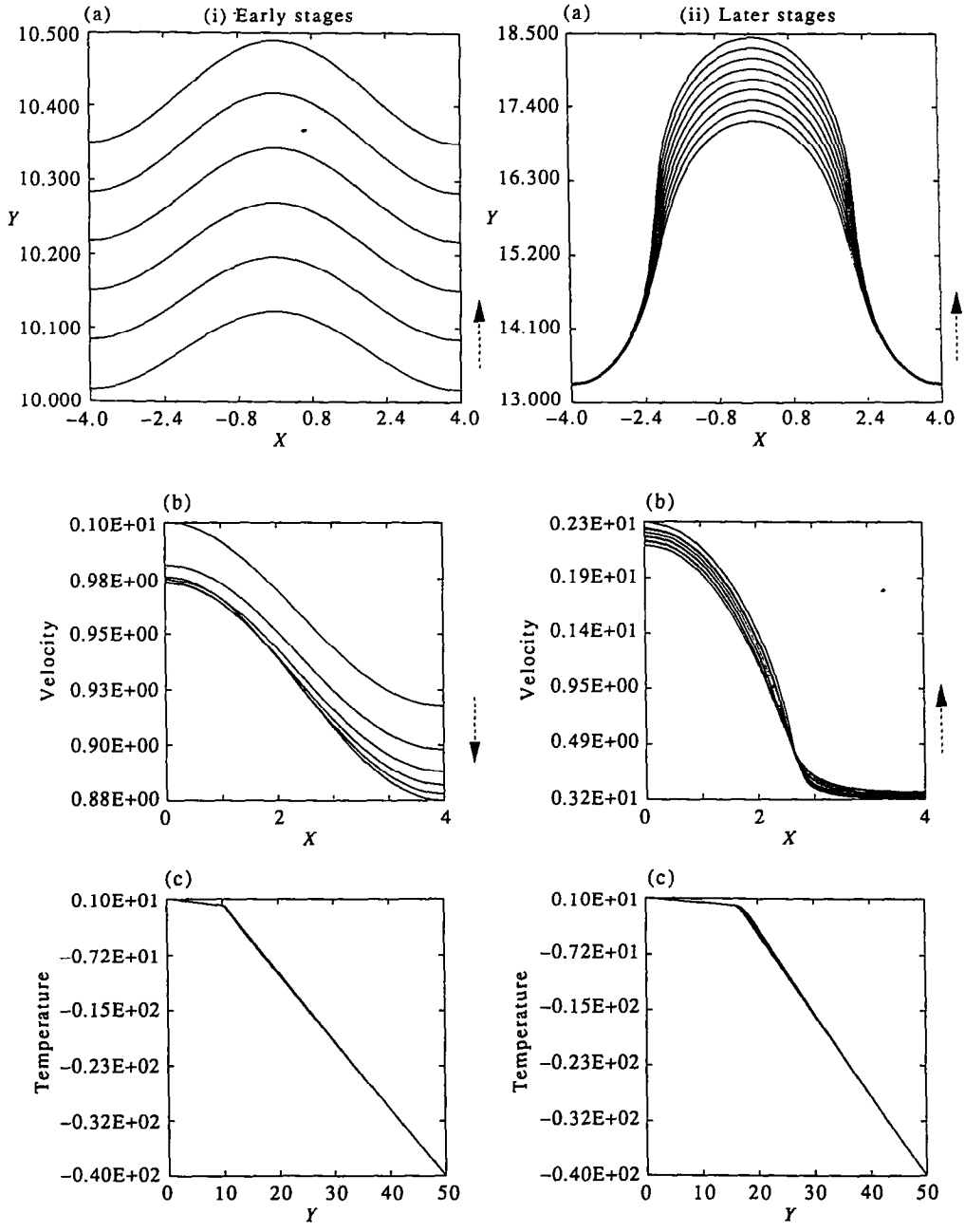

FIG. 6. Development of perturbed interface with surface tension $\gamma = 0.2$. Arrows show sequence of development. Only the right half was calculated. (i) Early stages of growth: (a) interface shape after reflection of the half computed. (b) Velocity of the right half. (c) Temperature profile at $X = 2$ in the two phases. (ii) Later stages of growth. (a), (b) and (c) as above.

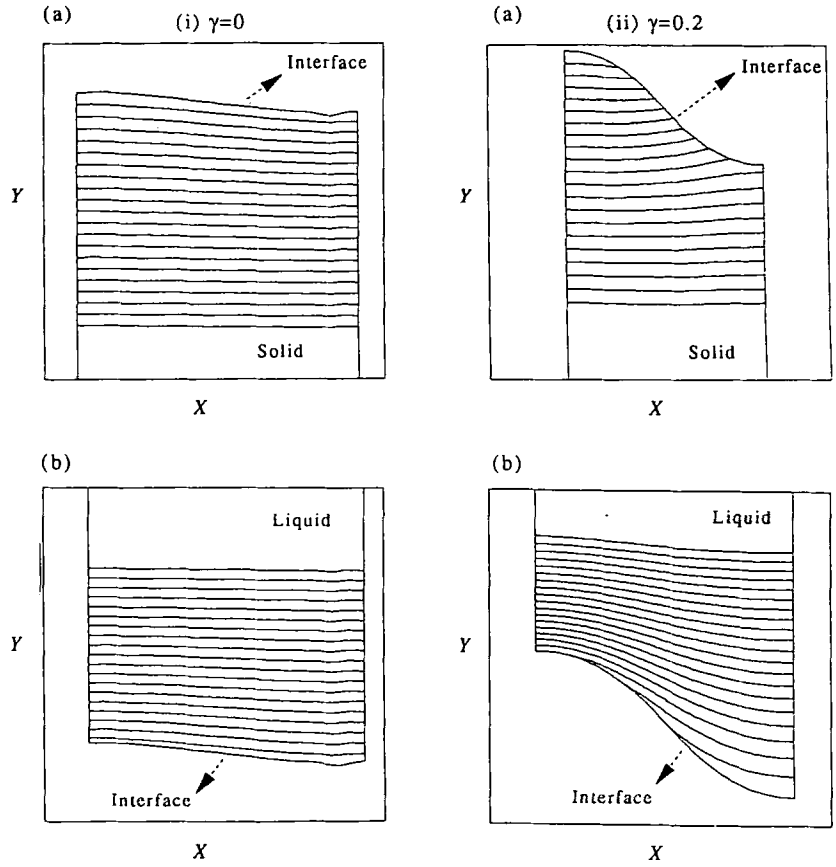

FIG. 7. Temperature contours in the two phases close to the interface. Contours in the solid are shown only in the range 0–0.3. In the liquid for 0 to −3. For the case of $\gamma = 0$, the interface is an isotherm. For $\gamma = 0.2$, the isotherms cross the interface. (i) Case without surface tension. (a) Contours in the solid. (b) Contours in the liquid. (ii) Case with surface tension $\gamma = 0.2$. (a) Contours in the solid. (b) Contours in the liquid.

initial shape of the perturbation. The mean position of the interface at the final stages of the development shown is at $Y = 11.2$ for the interface originally positioned at $Y = 10$. Thus the interface does not progress very far along the Y direction before exhibiting tip-splitting and cusp formation. It is also noticed that even in the initial stages the development of the cusp is indicated as seen from the interface velocity plot, shown for the half-wave calculated, in Fig. 5(iib). While leading to tip-splitting, from Fig. 5(iic), some regions on the interface are travelling faster than their adjacent points. These perturbations will again form distinct proturberances and propagate further until splitting occurs. Also shown in Figs. 5(ic) and 5(iic) are the temperature profiles in the solid and liquid regions at the initial and final stages, respectively. Obviously, the interface, corresponding to the discontinuity in the temperature gradient, has not progressed significantly before the instability occurs.

The application of surface tension of value $\gamma_{\text{eff}} = 0.2$ modifies the interfacial temperature through equation (23). In this case the interface development has been computed, and lies in strong contrast with results in the absence of surface tension. For such a low value of surface tension the interfacial temperature assumes values of the order of only $O(10^{-2})$. However, this is sufficient to permit the growth of the perturbation without the formation of cusps to significant amplitudes, as shown in Fig. 6(iia). Initially, the entire interface moves upward with speeds that are of the same order. In fact, there is an initial transient, for the given initial conditions, when the interface velocity actually decreases. This is shown in Fig. 6(ib). However, soon after, the velocity begins to increase again, especially at the tip. In the final stages of the evolution shown in Fig. 6(iia) however, the interfacial velocity, shown in Fig. 6(iib) is markedly different in two regions. In the region around the tip, the velocity is very much larger than at the sides. This is again due to the differences in temperature gradient between these regions. Regions of negative curvature are indeed warmer at the interface due to the Gibbs–Thomson effect. This is apparent from the temperature contour plots shown in Fig. 7, where the isotherms in the liquid are much

farther in the region of negative curvature, i.e. at the sides. This effect, of the interface slowing down strongly in the regions near the trough, has also been observed by DeGregoria and Schwartz [5] in their simulations of the Saffman–Taylor fingering phenomenon. With surface tension, the interface has progressed considerably in contrast to the case without. In fact the mean interface position now is at $Y = 16$ compared to 11.2 in the previous case. The initial amplitude to wavelength ratio of the perturbation is 0.0125 as in the zero surface tension case above. Here, the protuberance has grown to nearly 50 times its original size, in contrast with the previous case. This case illustrates the subtle effect that surface tension provides in modifying the stability characteristics of the phase interface. When the perturbation is in the embryonic stage, the surface tension influences the interface temperature only slightly (10^{-2}). Thus it prevents any formation of strong curvatures. However, as the protuberance grows, surface tension has an increasing effect on interfacial temperature and begins to influence the overall shape and velocity of the finger. It is noted that the growth rate of the perturbation depends on the surface tension since the tip curvature of a bump on the solid is controlled by the capillary length scale. In fact, increasing the value of surface tension for the cases mentioned above leads to the attenuation rather than growth of the initial perturbation.

5. CONCLUSIONS

The following conclusions may be arrived at from the preceding.

(1) The quasi-stationary approximation for interface motion is found to be inaccurate in capturing phase boundaries for higher Stefan numbers. With the full treatment, the temperature field, interface calculation and grid movement all interact over each iteration and time step. Such a computational method results in close agreement with analytical results for an isothermal interface.

(2) A generalised interface motion technique is developed, which is not limited to a single-valued or isothermal interface, and produces results in close agreement with analytical solutions for the one-phase and two-phase cases.

(3) The spatio–temporal development of deformed interfaces, with the allowance of the Gibbs–Thomson effect due to surface tension, is in line with theory. Tip-splitting and cusp formation are observed in the absence of surface tension. Addition of a small amount of surface tension completely changes the picture and a propagating finger is obtained for the duration computed. The shape and behaviour of the finger are in qualitative agreement with other investigators [5, 18–21] of analogous phenomena.

In summary, an interface tracking method has been developed and applied to study the materials solidification process. In conjunction with the scaling procedure adopted, significant morphological development has been achieved in a computationally efficient manner. The results obtained show clearly the effects of the competing mechanisms on the stability of a perturbed interface. The method will be useful in elucidating the various aspects of the phase change process.

Acknowledgements—The authors are pleased to acknowledge the partial support of GE Aircraft Engines and NASA Space Grant during the course of the present research. Helpful discussions with Drs D. G. Backman, D. Y. Wei and Y. Pang are appreciated.

REFERENCES

1. J. S. Langer, Instabilities and pattern formation in crystal growth, *Rev. Mod. Phys.* **52,** 1–28 (1980).
2. U. Nakaya, *Snow Crystals.* Harvard University Press, Cambridge, MA (1954).
3. J. Crank, *Free and Moving Boundary Problems.* Clarendon Press, Oxford, U.K. (1984).
4. L. N. Brush and R. F. Sekerka, A numerical study of two-dimensional crystal growth forms in the presence of anisotropic growth kinetics, *J. Crystal Growth* **96,** 419–441 (1989).
5. A. J. DeGregoria and L. W. Schwartz, A boundary-integral method for two-phase displacement in hele-shaw cells, *J. Fluid Mech.* **164,** 383–400 (1986).
6. G. B. McFadden and S. R. Coriell, Nonplanar interface morphologies during unidirectional solidification, *J. Crystal Growth* **84.** 371–388 (1987).
7. L. H. Ungar and R. A. Brown, Cellular interface morphologies in directional solidification. The one-sided model, *Phys. Rev. B.* **29**(3), 1367–1380 (1984).
8. R. Brower, D. Kessler, J. Koplik and H. Levine, Geometric approach to moving-interface dynamic, *Phys. Rev. Lett.* **51,** 1111–1114 (1983).
9. J. M. Floryan and H. Rasmussen, Numerical methods for viscous flows with moving boundaries, *Appl. Mech. Rev.* **42,** No. 12 (1989).
10. M. E. Thompson and J. Szekely, Density stratification due to counterbuoyant flow along a vertical crystallisation front, *Int. J. Heat and Mass Transfer* **32,** 1021–1036 (1989).
11. M. Lacroix, Computation of heat transfer during melting of a pure substance from an isothermal wall, *Numer. Heat Transfer, Part B* **15,** 191–210 (1989).
12. P. Pelce, *Dynamics of Curved Fronts, Perspectives in Physics.* Academic Press, New York (1988).
13. S.-C. Huang and M. E. Glicksman, Fundamentals of dendritic solidification—I. Steady-state tip growth, *Acta Metall.* **29,** 701–715 (1981). Fundamentals of dendritic solidification—II. Development of sidebranch structure, *Acta Metall.* **29,** 717–734 (1981).
14. J. F. Thompson, Z. U. A. Warsi and C. W. Mastin, *Numerical Grid Generation.* Elsevier, New York (1985).
15. W. Shyy, Y. Pang, G. B. Hunter, D. Y. Wei and M.-H. Chen, Modelling of turbulent transfport during continuous ingot casting, *Int. J. Heat Mass Transfer* **35,** 1229–1245 (1992).
16. C. Herring, Surface tension as a motivation for sintering. In *Physics of Powder Metallurgy* (Edited by W. E. Kingston), pp. 143–179. McGraw Hill, New York (1951).
17. W. Shyy, An adaptive grid method for Navier–Stokes

flow computation, *Appl. Math. Comput.* **21**, 201–219 (1987).
18. D. Bensimon and P. Pelce, Tip-splitting solutions to a Stefan problem, *Phys. Rev.* **A33**, 4477–4478 (1986).
19. D. Bensimon, Stability of viscous fingering, *Phys. Rev.* **A33**, 1302–1308 (1986).
20. D. A. Kessler, J. Koplik and H. Levine, Pattern selection in fingered growth phenomenon, *Adv. Phys.* **37**(3), 255–339 (1988).
21. S. D. Howison, J. R. Ockendon and A. A. Lacey, Singularity development in moving-boundary problems, *Q. Jl Mech. Appl. Math.* **38**(3), 343–360 (1985).